THE JOURNAL OF PHYSICAL CHEMISTRY C

Article

pubs.acs.org/JPCC

Linear and Hexagonal Porous Structures of an Organic Charge Acceptor Hexaaza-triphenylene-hexacarbonitrile on Au(111) with CN···CN Dipolar Interactions

Sang-Yeon Won,[†,§] Ji-Hoon Kim,[‡,§] Howon Kim,[†] Jong Keon Yoon,[†] Se-Jong Kahng,*[,†] Young-Kyun Kwon,*[,‡] and Yongsup Park*[,‡]

[†]Department of Physics, Korea University, 136-713, Seoul, Republic of Korea

[‡]Department of Physics and Research Institute for Basic Sciences, Kyung Hee University, 130-701, Seoul, Republic of Korea

ABSTRACT: Knowledge of molecular structures of emerging charge acceptors, such as hexaaza-triphenylene-hexacarbonitrile (HATCN), on metal surfaces is essential for their optoelectronic device applications. Here, we studied the two-dimensional molecular ordering of HATCN at submonolayer coverages on Au(111) using scanning tunneling microscopy (STM). Linear and hexagonal porous structures were observed at atomic steps and terraces, respectively, and our density functional theory calculations revealed that the structures were stabilized with CN···CN dipolar interactions. The hexagonal porous structures possess chirality, and they form only small (<1000 nm^2) phase-separated chiral domains that easily change their structures in subsequent STM images at 80 K, which explains the no electron diffraction pattern reported previously.

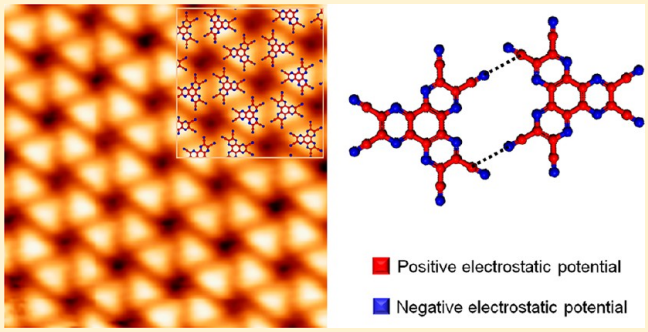

INTRODUCTION

Thin organic layers on metal substrates have attracted considerable interest due to their possible applications in organic (opto-)electronic devices, such as organic light-emitting diodes (OLEDs), photovoltaic cells (OPVCs), and field effect transistors (OFETs).[1−4] Molecules in organic layers donate and accept electrons to and from metal subtrates, respectively, changing the work functions of the substrates. Especially, these mechanisms allow continuous tuning of electron and hole numbers that recombine (are saperated) to emit (by adsorption of) photons in OLEDs (OPVCs), thereby affecting their quantum efficiency. The quantum efficiency can be optimized by experimenting with various molecules, coverages, and interface structures, which strongly promoted the efforts to understand the geometric and electronic properties of molecular layers on metal substrates.[5−7]

The hexaaza-triphenylene-hexacarbonitrile (HATCN) molecule is a promising molecular acceptor due to its extremely high ionization energy (9.2 eV) and thermal stability with large molecular weight (384.29 amu), compared with a widely studied acceptor, tetrafluoro-tetracyanoquinodimethane (F4-TCNQ).[8−11] The growth and electronic behaviors of HATCN molecules have been recently studied on coinage metal surfaces, including Au(111) using various techniques, atomic force microscopy (AFM), thermal desorption spectroscopy (TDS), low-energy electron diffraction (LEED), X-ray diffraction (XRD), and X-ray photoelectron spectroscopy (XPS).[12,13] It was argued that HATCN molecules adsorbed flat lying on the Au(111) surface without considerable lateral interactions between the molecules up to 0.5 monolayer (ML) and that, with increasing coverage (between 0.5 and 1 ML), repulsive dipole interactions arose between them.[12] It was also reported that no LEED pattern could be obtained for the first layer, even at liquid nitrogen temperature, due to the high mobility of the molecules on the Au(111) surface.[13] However, there has been no report available in the literature that visualizes these growth models at the single molecule level on the Au(111) surface.[8]

In this paper, we report on the intermolecular structures of HATCN molecules on Au(111), studied using a scanning tunneling microscope (STM). In contrast to previous models, locally ordered molecular structures were observed both below 0.5 ML and between 0.5 and 1 ML. Molecular models for the observed structures were proposed and reproduced with density functional theory (DFT) calculations. We argued that two HATCN molecules in the ordered structures were under attractive, instead of repulsive, dipolar CN···CN interactions.

EXPERIMENTAL SECTION

STM experiments were performed using a home-built STM housed in an ultra-high-vacuum (UHV) chamber with a base pressure < 7×10^{-11} Torr. The Au(111) surface was prepared from a thin film (200 nm thick) of Au on mica that was cleaned by several cycles of Ne-ion sputtering and annealing at 800 K. The surface cleanliness of the Au(111) was checked by

Received: July 19, 2013
Revised: September 15, 2013
Published: September 20, 2013

   dx.doi.org/10.1021/jp407173w | J. Phys. Chem. C 2013, 117, 21371−21375

observing typical herringbone structures on the terraces in the STM images. Commercially available HATCN was thermally evaporated on the Au(111) surface at submonolayer coverage from an alumina-coated crucible, keeping the substrate temperature at 150 K. The HATCN material was outgassed for several hours prior to deposition, and the molecular flux was about 0.1/nm^2·min. The prepared sample was transferred to the STM and cooled down to 80 K. A Pt−Rh alloy tip was used as the STM probe.

THEORETICAL CALCULATIONS

To verify the two-dimensional molecular ordering of HATCN, we performed first-principles density-functional calculations using the VASP code.[14,15] Interaction between ions and electrons was approximated by the projector-augmented wave potential.[16] A generalized gradient approximation (GGA) with the Perdew−Burke−Ernzerhof (PBE) functional was used to describe the exchange correlations between electrons.[17] For the plane-wave expansion and the surface-Brillouin-zone integration, we used the cutoff energy of 400 eV and only the Γ point, respectively, which turned out to be sufficient to get converged results. To describe nonbonding interactions between the molecules, particularly of the van der Waals type, an empirical correction scheme proposed by Grimme was adopted.[18] The height of the simulation box perpendicular to the molecule plane was fixed at 20 Å to avoid an artificial interaction from neighboring slabs. The dipole-correction scheme was also applied to compensate the imaginary dipoles of neighboring slabs. The energy for an isolated molecule, as a reference, was obtained using a 25 × 25 × 20 Å^3 supercell.

RESULTS AND DISCUSSION

HATCN is a planar molecule with four conjugate rings terminated with six CN ligands, as shown in Figure 1a. The electrostatic potential distribution shown in Figure 1a was calculated using DFT methods based on the generalized gradient approximation (GGA) and mapped on the isosurfaces of 0.003 e/Bohr^3. C and N atoms showed positive and negative electrostatic potential, reflecting their electronegativities, 2.55 and 3.04, respectively. HATCN molecules had a large enough surface diffusivity to form cluster structures when they were deposited at 150 K on Au(111). After deposition, the sample was cooled to 80 K to perform the STM measurement, and a typical STM image obtained from HATCN on Au(111) at 0.2 ML is shown in Figure 1b. A single molecule was identified as a triangular shape in STM images. At atomic step edges, the molecules formed two chain structures, running parallel to each other, at upper and lower parts of steps in Figure 1c. Diffusion barriers at step edges provide stable adsorption sites at both parts of steps. At terraces, molecular clusters form preferably at the face-centered cubic (fcc) regions of Au(111) herringbone reconstructions. It has been reported that fcc regions provide active adsorption sites for atoms and molecules on Au(111) owing to their low surface atom density, in comparison with hexagonal close-packed (hcp) regions and dislocation ridges.[19−22] In the molecular clusters, hexagonal porous (HP) structures are visible as well as loosely packed structures in Figure 1b,d.

As molecular coverage increased, the HP structures became dominant structures on the surface. Panels (a) and (b) in Figure 2 show typical STM images obtained after the deposition of 0.7 ML HATCN on Au(111). A molecular

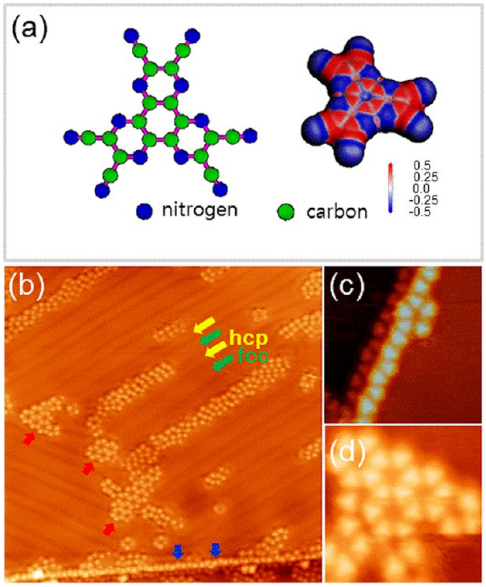

Figure 1. (a) A molecular model and a calculated molecular electrostatic potential distribution (in volts) of hexaaza-triphenylene-hexacarbonitrile (HATCN) molecules at isodensity surfaces, shown in red (positive) and blue (negative). (b) A typical scanning tunneling microscopy (STM) topography image obtained at 80 K after 0.2 monolayer (ML) of HATCN molecules was deposited on Au(111) at 150 K. Yellow and green arrows indicate hexagonal close-packed (hcp) and face-centered cubic (fcc) regions of herringbone reconstructions of bare Au(111), respectively. Red and blue arrows indicate hexagonal porous and linear strucutres, respectively. Higher-resolution STM images obtained in similar regions showing (c) linear structures and (d) hexagonal porous (HP) structures made of HATCN. Sizes of STM images: (b) 90 × 90 nm^2, (c) 15 × 15 nm^2, (d) 8 × 8 nm^2. Sample voltages: (b, c) V_S = 1 V, (d) V_S = 0.8 V. Tunneling current I_T = 0.1 nA for all images.

model was superimposed to the STM images in Figure 2b. To identify intermolecular interactions in the HP structures, the configuration of two neighboring molecules are drawn in Figure 2c, with the simplified version of electrostatic potential distributions at C and N based on the single molecule potential distributions of Figure 1a. Two neighboring HATCN molecules have two possible intermolecular bonds in the HP structures, as denoted with dotted lines in Figure 2c. It can be deduced that the two intermolecular bonds between two CN ligands originate from dipolar interactions. The configuration of two neighboring molecules in HP is applicable to understand the linear structures observed at step edges. Two neighboring HATCN molecules in the linear structures form similar configurations to those in HP, implying that the linear structures are also made of dipolar interactions.

DFT calculations were performed to understand the precise arrangement of HATCN molecules in HP structures. A hexagonal unit cell containing two HATCN molecules as the basis was used to describe the periodic structures, as depicted in Figure 3a. We considered the lattice constant L and the relative angle θ of a molecular axis with respect to a lattice vector, as two independent parameters. We approximated that the two molecules in a unit cell shared the parameter θ for their angular configurations. The calculation results are displayed with the formation energy in color code as functions of L and θ as shown in Figure 3b. Three stable molecular configurations are visible. Our experimental observations, L = 1.9 nm and θ = 15°,

dx.doi.org/10.1021/jp407173w | J. Phys. Chem. C 2013, 117, 21371−21375

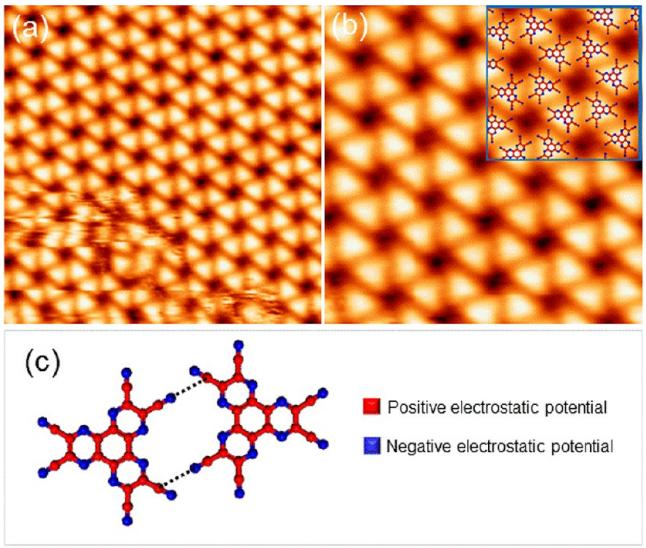

Figure 2. (a) A typical STM topography image obtained at 80 K after 0.7 ML of HATCN molecules was deposited at 150 K. (b) High-resolution STM images from (a) with molecular models partly superimposed over the image. (c) Schematic illustrations for two nearest-neighbor HATCN molecules with simplified electrostatic potential distributions. Positive and negative potential distributions are represented with red and blue colors, respectively. Dotted lines indicate possible intermolecular bonds C···N. Sizes of STM images: (a) 23.5 × 23.5 nm^2, (b) 16 × 16 nm^2. Sample voltages: (a) V_S = 1 V, (b) V_S = 1.5 V. Tunneling current I_T = 0.1 nA for all images.

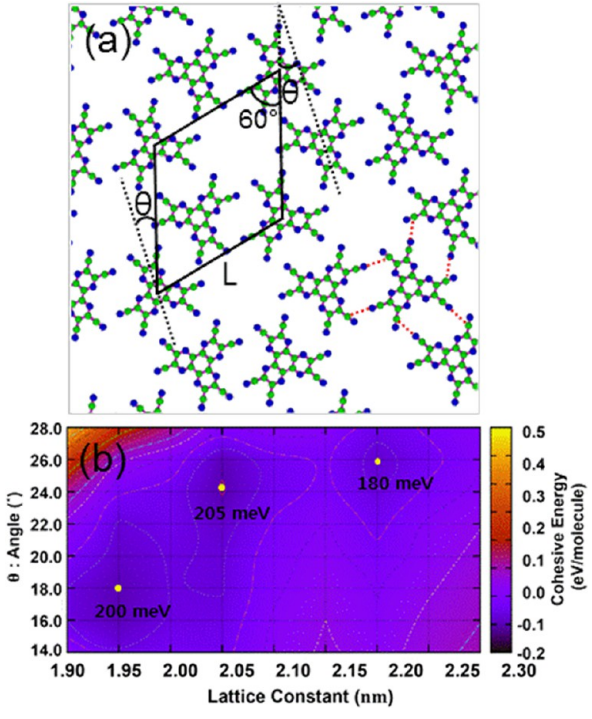

Figure 3. (a) The relaxed HP structures of HATCN obtained from density functional theory calculations. Hexagonal unit cells with three possible intermolecular interactions per molecule are drawn with dotted lines. (b) The cohesive energy per molecule as a function of a lattice parameter L and an angle θ depicted in (a), respectively. Three stable molecular configurations are visible.

show reasonable agreements with the second stable configuration, L = 1.95 nm and θ = 18.0°. In fact, similar HP structures were observed on Ag(111) with a 7 × 7 superstructure[8] with L = 2.02 nm, which matched well with the most stable configuration, L = 2.02 nm and θ = 24.2°. Since the calculation results L = 1.95 nm and θ = 18.0° well-reproduce the model in Figure 2, the length of possible intermolecular bonds considered in Figure 2b,c is extracted from the calculation results. The CN···CN distance was 0.366 nm, which is a little bit larger than the sum of van der Waals radii for C (0.170 nm) and N (0.155 nm), but still close to it, implying that the dipolar CN···CN interaction would be the mechanism that stabilized HP structures. From our DFT calculations, we obtained the energy gain of 200 meV per molecule. Because one molecule forms three CN···CN intermolecular bonds in HP structures, each bond carries roughly a 70 meV energy gain.

Even though HATCN molecules do not possess chirality, the HP structures do have chirality. Panels (a) and (b) in Figure 4

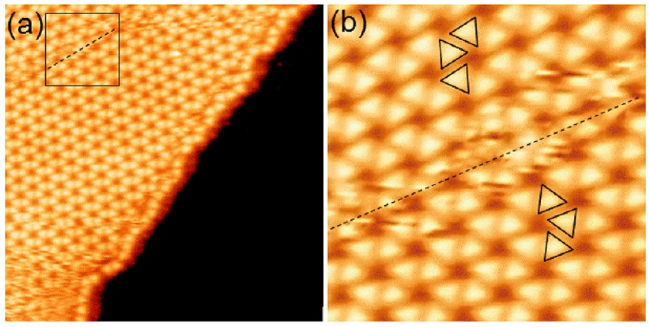

Figure 4. (a) A typical STM topography image obtained at 80 K after 0.7 ML of HATCN molecules was deposited at 150 K. (b) High-resolution STM images from (a). Domain boundary is denoted with a dotted line. Three molecules are overlaid with triangles at upper and lower domains to signify their chiral structures. Sizes of STM images: (a) 55.5 × 55.5 nm^2, (b) 12.5 × 12.5 nm^2. Sample voltages: (a) V_S = 1 V, (b) V_S = 1.5 V. Tunneling current I_T = 0.1 nA for all images.

show two different domains of HP structures, at the upper and lower parts of the image. The upper part shows clockwise HP structures (λ-domains), whereas the lower part shows anticlockwise HP structures (δ-domains), as depicted in Figure 4b. They are separated by a fuzzy domain boundary, at which HATCN molecules seem to be mobile. We observed that not only domain boundaries but also molecular domains were fluctuating at some regions even at 80 K. Figure 5 shows STM images obtained subsequently at the same location with a 0, 3,

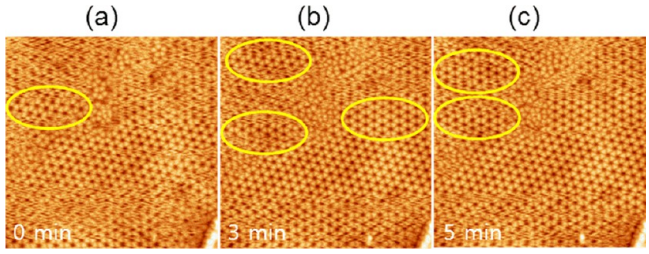

Figure 5. (a–c) STM topography images subsequently obtained from the same region with the time delay of 0, 3, and 5 min at 80 K. The small domains that change in the following images are denoted with yellow marks. Size of STM images: 58 × 58 nm^2, for (a)–(c). Sample voltages: (a) V_S = 1 V, (b) V_S = 1.5 V. Tunneling current I_T = 0.1 nA for all images.

dx.doi.org/10.1021/jp407173w | J. Phys. Chem. C 2013, 117, 21371–21375

and 5 min delay. Some small domains in Figure 5 appear and disappear as time goes on. This domain fluctuation can be caused by the interactions between the STM tip and molecules. Poor lateral resolution at the regions between molecular domains can be an indicator for tip instability due to the interactions. Another way to understand this behavior is to find a connection with the previous LEED results; no LEED pattern and a 7 × 7 LEED pattern were observed on Au(111) and Ag(111), respectively.[13] Even if both have 0.288 nm lattice constants, atomic structures of bare Au(111) and Ag(111) surfaces are different. The well-known 22 × $\sqrt{3}$ herringbone reconstructions form only on Au(111). In the case of Ag(111), the 0.288 nm lattice constant and the 2.02 nm HP structure lattice are commensurate, which explains why a 7 × 7 LEED pattern could be observed in this system. In the case of Au(111), however, the reduced and varying lattice constant due to herringbone reconstructions may not allow a commensuration condition with either 2.02 or 1.95 nm obtained in our calculations. Because of such ill-matched relations between HP structures and herringbone reconstructions, HP domains remained small, not exceeding 1000 nm^2, and embedded in disordered structures. Some molecules are even mobile in the disordered structures and form new HP domains, as shown in Figure 5. Although it is hard to rule out the possibility that the domain fluctuation is influenced by the STM tip, the small domains under dynamic fluctuations can explain the no LEED pattern reported previously.[13] Our DFT calculations did not include underlying Au(111). Obviously, HATCN molecules interact with Au(111) to some extent, as revealed by the adsorption selectivity for fcc regions in 0.2 ML results. Significant charge transfer from Au(111) to HATCN molecules will appear in DFT calculations including the Au(111) substrate.

CONCLUSIONS

We studied the molecular structures of HATCN at submonolayer coverages on Au(111) using STM. Linear and hexagonal porous structures were observed at atomic steps and terraces of Au(111), respectively. Molecular models for the observed structures were proposed and reproduced DFT calculations. The HP structures are stabilized with three CN···CN dipolar interactions per molecule. The HP structures possess chirality, forming phase-separated chiral domains that easily change their structures in subsequent STM images at 80 K.

AUTHOR INFORMATION

Corresponding Authors

*E-mail: sjkahng@korea.ac.kr. Tel: (+82) 2-3290-3109. Fax: (+82) 2-922-3484.

*E-mail: ykkwon@khu.ac.kr. Tel: (+82) 2-961-9279. Fax: (+82) 2-957-8408.

*E-mail: parky@khu.ac.kr. Tel: (+82) 2-961-0729. Fax: (+82) 2-957-8408.

Author Contributions

§These authors equally contributed to this work.

Notes

The authors declare no competing financial interest.

ACKNOWLEDGMENTS

We gratefully acknowledge financial support from the Ministry of Education Science and Technology of the Korean government through the National Research Foundation (Grant nos. 2011-0015172; 2011-0016188; 2012-0013222). This study was supported by the Supercomputing Center/Korea Institute of Science and Technology Information with supercomputing resources including technical support (KSC-2012-C2-72 and KSC-2013-C2-024).

REFERENCES

(1) Kymissis, I. *Organic Field Effect Transistors: Theory, Fabrication and Characterization*; Springer Science; New York, 2009.

(2) Komp, R. J. *Practical Photovoltaics: Electricity from Solar Cells*; Aatec Publications: Ann Arbor, MI, 2001.

(3) Tsujimura, T. *OLED Display Fundamentals and Applications*; John Wiley & Sons: Hoboken, NJ, 2012.

(4) Forrest, S. R.; Thompson, M. E. Introduction: Organic Electronics and Optoelectronics. *Chem. Rev.* **2007**, *107*, 923−925.

(5) Koch, N. Organic Electronics Devices and Their Functional Interfaces. *ChemPhysChem* **2007**, *8*, 1438−1455.

(6) Ishii, H.; Sugiyama, K.; Ito, E.; Seki, K. Energy Level Alignment and Interfacial Electronic Structures at Organic/Metal and Organic/Organic Interface. *Adv. Mater.* **1999**, *11*, 605−625.

(7) Baldo, M. A.; Forrest, S. R. Interface-Limited Injection in Amorphous Organic Semiconductors. *Phys. Rev. B* **2001**, *64*, 085201.

(8) Glowatzki, H.; Bröker, B.; Blum, R. P.; Hofmann, O. T.; Vollmer, A.; Rieger, R.; Müllen, K.; Zojer, E.; Rabe, J. P.; Koch, N. "Soft" Metallic Contact to Isolated C_{60} Molecules. *Nano Lett.* **2008**, *8*, 3825−3829.

(9) Kim, Y. K.; Kim, J. W.; Park, Y. Energy Level Alignment at a Charge Generation Interface Between 4,4′-bis(*N*-phenyl-1-naphthylamino)biphenyl and 1,4,5,8,9,11-hexaazatriphenylene-hexacarbonitrile. *Appl. Phys. Lett.* **2009**, *94*, 063305.

(10) Liao, L. S.; Slusarek, W. K.; Hatwar, T. K.; Ricks, M. L.; Comfort, D. L. Tandem Organic Light-Emitting Diode Using Hexaazatriphenylene Hexacarbonitrile in the Intermediate Connector. *Adv. Mater.* **2008**, *20*, 324−329.

(11) Liao, L. S.; Klubek, K. P. Power Efficiency Improvement in a Tandem Organic Light-Emitting Diode. *Appl. Phys. Lett.* **2008**, *92*, 223311.

(12) Frank, P.; Koch, N.; Koini, M.; Rieger, R.; Müllen, K.; Resel, R.; Winkler, A. Layer Growth and Desorption Kinetics of a Discoid Molecular Acceptor on Au(111). *Chem. Phys. Lett.* **2009**, *473*, 321−325.

(13) Frank, P.; Djuric, T.; Koini, M.; Salzmann, I.; Rieger, R.; Müllen, K.; Resel, R.; Koch, N.; Winkler, A. Layer Growth, Thermal Stability, and Desorption Behavior of Hexaaza-triphenylene-hexacarbonitrile on Ag(111). *J. Phys. Chem. C* **2010**, *114*, 6650−6657.

(14) Kresse, G.; Hafner, J. Ab Initio Molecular Dynamics for Liquid Metals. *Phys. Rev. B.* **1993**, *47*, 558−561.

(15) Kresse, G.; Hafner, J. Ab Initio Molecular-Dynamics Simulation of the Liquid-Metal−Amorphous-Semiconductor Transition in Germanium. *Phys. Rev. B.* **1994**, *49*, 14251.

(16) Blöchl, P. E. Projector Augmented-Wave Method. *Phys. Rev. B.* **1994**, *50*, 17953.

(17) Perdew, J. P.; Burke, K.; Ernzerhof, M. Generalized Gradient Approximation Made Simple. *Phys. Rev. Lett.* **1996**, *77*, 3865−3868.

(18) Grimme, S. Accurate Description of van der Waals Complexes by Density Functional Theory Including Empirical Corrections. *J. Comput. Chem.* **2004**, *25*, 1463−1473.

(19) Gong, J.; Ojifinni, R. A.; Kim, T. S.; White, J. M.; Buddie Mullins, C. Selective Catalytic Oxidation of Ammonia to Nitrogen on Atomic Oxygen Precovered Au(111). *J. Am. Chem. Soc.* **2006**, *128*, 9012−9013.

(20) Chen, W.; Madhavan, V.; Jamneala, T.; Crommie, M. F. Scanning Tunneling Microscopy Observation of an Electronic Superlattice at the Surface of Clean Gold. *Phys. Rev. Lett.* **1998**, *80*, 1469−1472.

(21) Gottschalck, J.; Hammer, B. A Density Functional Theory Study of the Adsorption of Sulfur, Mercapto, and Methylthiolate on Au(111). *J. Chem. Phys.* **2002**, *116*, 784.
(22) Wang, Y.; Hush, N. S.; Reimers, J. R. Simulation of the Au(111)-(22×$\sqrt{3}$) Surface Reconstruction. *Phys. Rev. B* **2007**, *75*, 233416.

dx.doi.org/10.1021/jp407173w | *J. Phys. Chem. C* 2013, 117, 21371−21375